Electronic Supplementary Material (ESI) for Nanoscale.

Supporting Information

Yolk-Shell Structured $CoSe_2$/C Nanospheres as Multifunctional Anode Materials for Both Full/Half Sodium-Ion and Full/Half Potassium-Ion Batteries

Xiuping Sun, [a] *Suyuan Zeng,* [b] *Ruxia Man,* [a] *Lu Wang* [a], *Bo Zhang,* [a] *Fang Tian,* [a] *Yanjun Zhai,* [b] *Yitai Qian* [a] *and Liqiang Xu** [a]

[a] Key Laboratory of Colloid and Interface Chemistry, Ministry of Education, School of Chemistry and Chemical Engineering, Shandong University, Jinan 250100, China.

E-mail: xulq@sdu.edu.cn.

[b] Shandong Provincial Key Laboratory / Collaborative Innovation Center of Chemical Energy Storage & Novel Cell Technology, Liaocheng University, China

Content

Figure Captions:

Fig. S1. The amount of $Co(NO_3)_2·6H_2O$ is (a) 0.7 mmol, (b) 0.5 mmol, (c) 0.3 mmol, (d) 0.2 mmol, (e) 0.1 mmol to form the cobalt glycerate solid spheres.

Fig. S2. The effect of nanosphere size on performances: when added cobalt salt 0.7 mmol, the size of nanosphere is about 980 nm and when added cobalt salt 0.2 mmol, the size of nanosphere is about 450 nm.

Fig. S3 (a, b) FESEM images (c) TEM image of Co-glycerate spheres.

Fig. S4 (a) FESEM image (b) TEM image of $CoSe_2$/C.

Fig. S5 (a) FESEM image (b) TEM image (c) EDX mapping images (Co, O) of Co_3O_4.

Fig. S6 XPS spectrum of $CoSe_2$/C.

Fig. S7 N_2 adsorption/desorption isotherms of Co_3O_4.

Fig. S8 TGA and DTA curves of (a) Co-glycerate spheres were annealed in air atmosphere, (b) Co-glycerate spheres were annealed in N_2 atmosphere.

Fig. S9 FESEM images of (a, b, c) Co-glycerate spheres were annealed in N_2 atmosphere at different temperature.

Fig. S10 XRD patterns of Co-glycerate spheres were annealed in N_2 atmosphere at different temperature.

Fig. S11 FESEM images of (a, b, c) Co-glycerate spheres were annealed in air atmosphere at different temperature.

Fig. S12 XRD patterns of Co-glycerate spheres were annealed in air atmosphere at different temperature.

Fig. S13 Raman spectrum of $CoSe_2$/C.

Fig. S14 (a) Charge-discharge curves of the first cycle at 100 mA g^{-1}, (b) ex-situ XRD patterns of $CoSe_2$/C for SIBs, SEM images of $CoSe_2$/C (c) discharge to 0.5 V, (d) charge to 2.9 V.

Fig. S15 Elemental mapping of $CoSe_2$/C after 100 cycles at 500 mA g^{-1} for SIBs.

Fig. S16 Cycling performance of $CoSe_2$/C at 1 A g^{-1} in SIBs.

Fig. S17 Cycling performance of $CoSe_2$/C at 8 A g^{-1} in SIBs.

Fig. S18 The cycling performances at 500 mA g^{-1} in different electrolyte for SIBs (a) 1 M $NaClO_4$ in EC: DEC (1:1 Vol%) containing 5 wt.% FEC and 1 M $NaPF_6$ in EC: DEC (1:1 Vol%) containing 2 wt.% FEC, the cycling performances at 100 mA g^{-1} (b) 0.8 M KPF_6 in EC: DEC (1:1 Vol%) was used as electrolyte for PIBs.

Fig. S19 (a) Electrochemical impedance spectra of $CoSe_2$/C and Co_3O_4 before cycle for SIBs, (b) The relationship between Z' and $\omega^{-1/2}$ for $CoSe_2$/C and Co_3O_4 in the low-frequency region.

Fig. S20 (a) XRD pattern, (b) FESEM image of $Na_3V_2(PO_4)_3$@rGO.

Fig. S21 (a) The working principle of SIBs full-cell with a $CoSe_2$/C anode and a $Na_3V_2(PO_4)_3$@rGO cathode, (b) charge-discharge curves of the 1st cycle at 1A g^{-1}, (c) rate performance, (d) cycling performances of $CoSe_2$/C//$Na_3V_2(PO_4)_3$@rGO in SIBs full-cell at1 A g^{-1}.

Fig. S22 Charge-discharge curves of $CoSe_2$/C at 50 mA g^{-1} in PIBs.

Fig. S23 When the mass load of $CoSe_2$/C was 6.3 mg cm^{-2} for potassium ion battery, charge-discharge curves at 50 mA g^{-1}.

Fig. S24 Comparison the performance of $CoSe_2$/C with recently reported materials in PIBs.

Fig. S25 FESEM images of (a) PTCDA, (b) PTCDA-450, (c) XRD patterns of PTCDA and PTCDA-450.

Fig. S26 Photos of disassembled battery after cycling (a) the electrode of PTCDA-450, (b) the side of separator contact with PTCDA-450 electrode directly, (c) the other side of separator, (d) the cycling performance of PTCDA-450 at 100 mA g^{-1} in half potassium ion battery.

Fig. S27 The charge-discharge curves of $CoSe_2$/C//PTCDA-450 of the first cycle at 100 mA g^{-1} in PIBs full-cell.

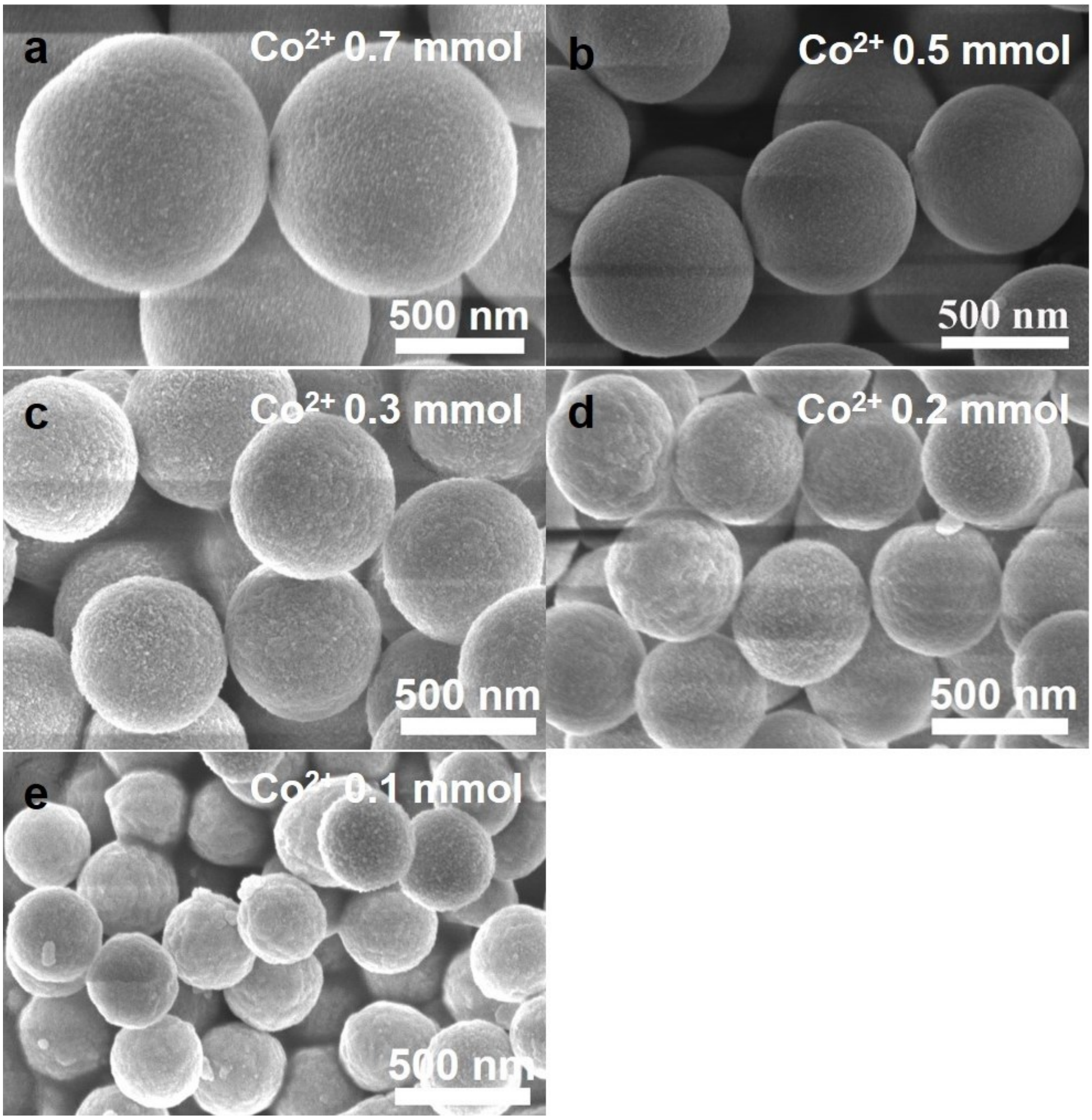

Fig. S1 the amount of $Co(NO_3)_2 \cdot 6H_2O$ is (a) 0.7 mmol, (b) 0.5 mmol, (c) 0.3 mmol, (d) 0.2 mmol, (e) 0.1 mmol to form the cobalt glycerate solid spheres.

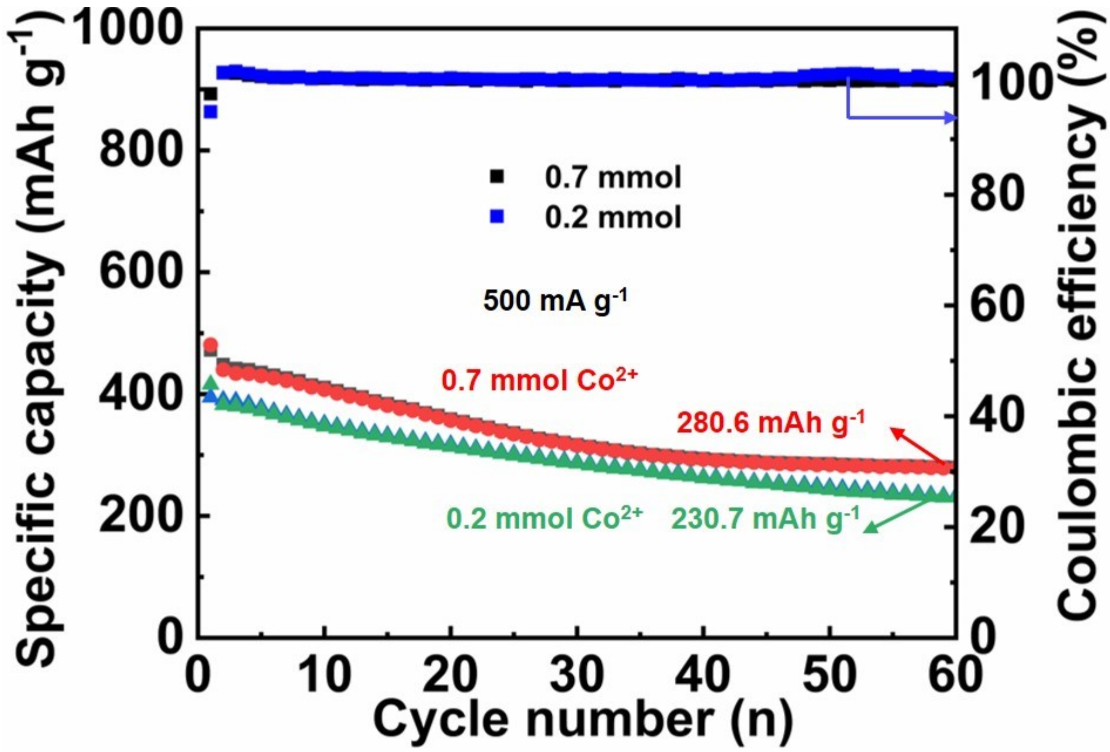

Fig. S2 The effect of nanosphere size on performances: when added cobalt salt 0.7 mmol, the size of nanosphere is about 980 nm and when added cobalt salt 0.2 mmol, the size of nanosphere is about 450 nm.

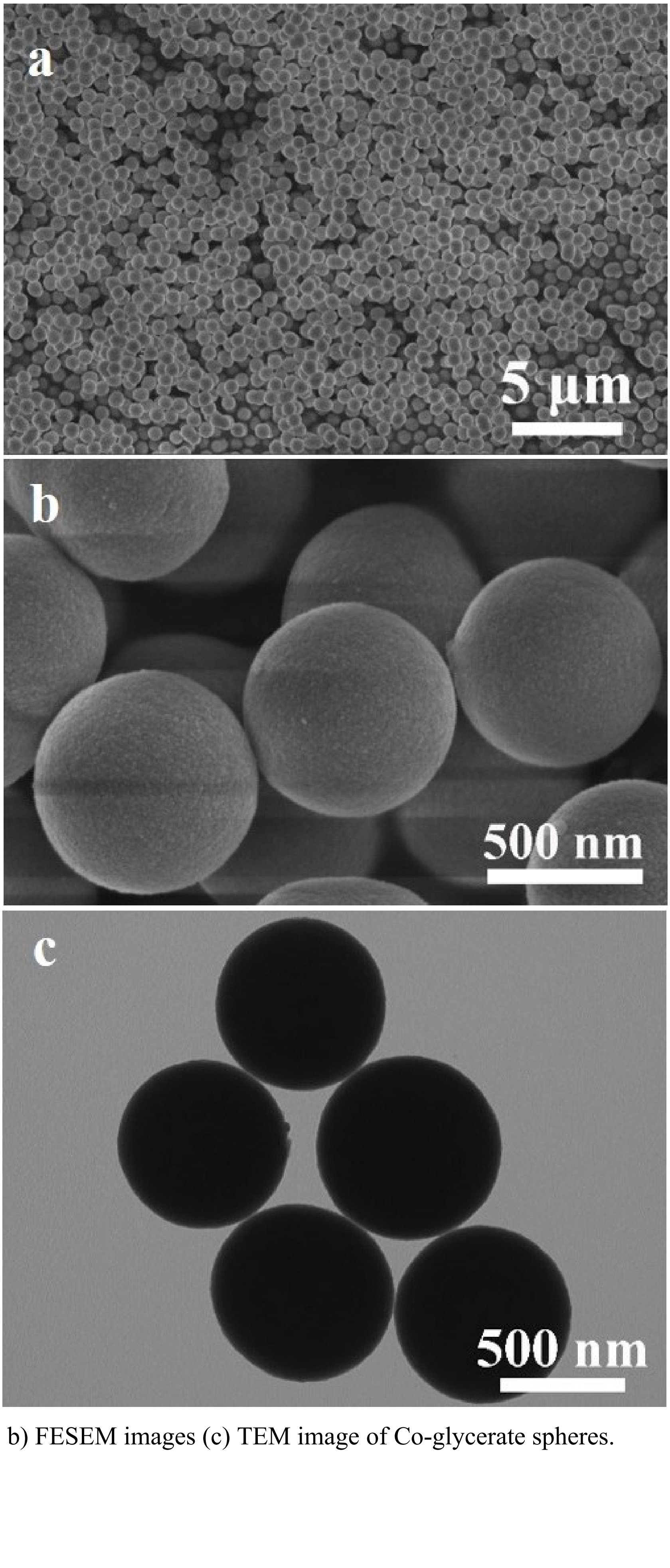

Fig. S3 (a, b) FESEM images (c) TEM image of Co-glycerate spheres.

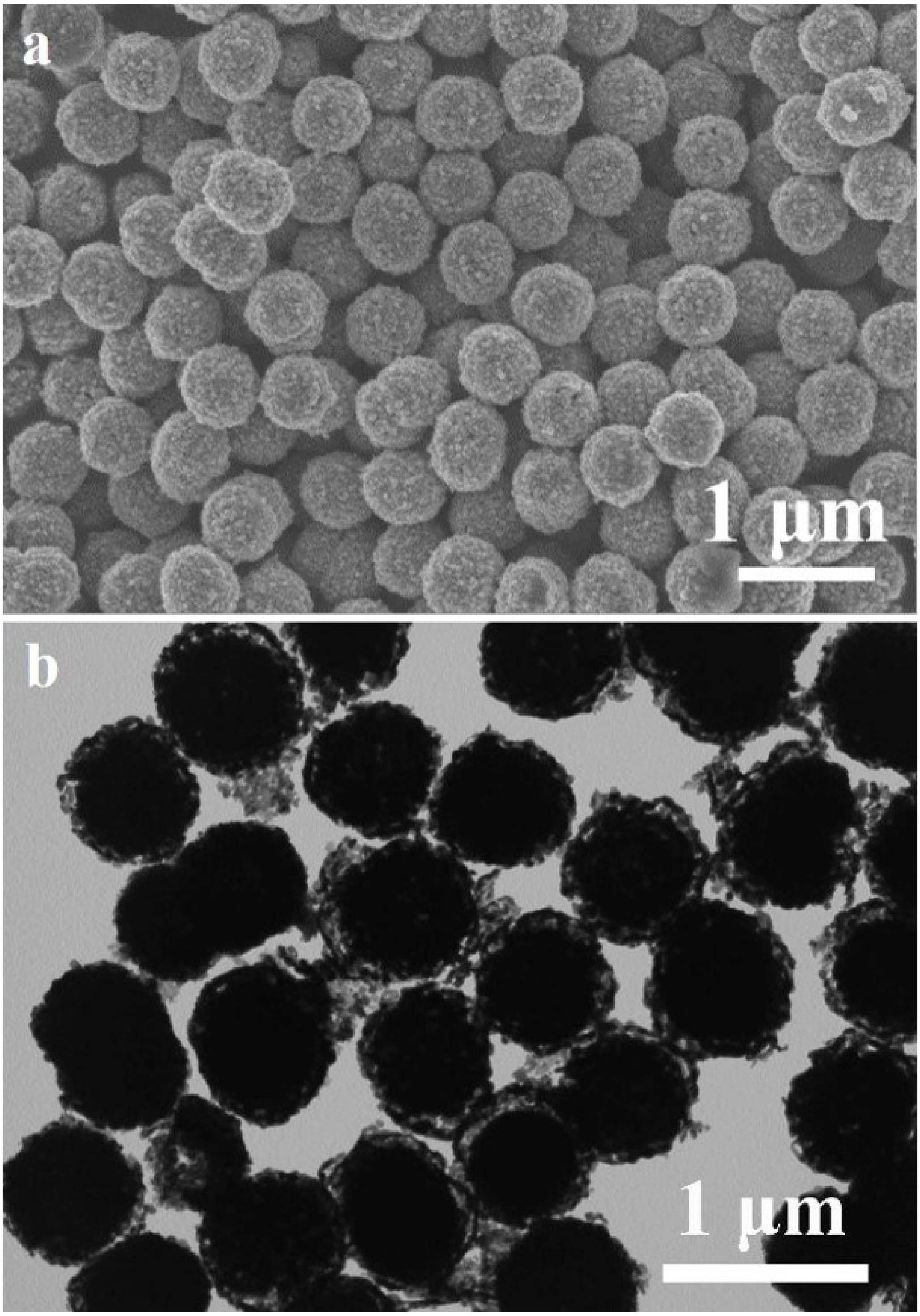

Fig. S4 (a) FESEM image (b) TEM image of $CoSe_2/C$.

Fig. S5 (a) FESEM image (b) TEM image (c) EDX mapping images (Co, O) of Co_3O_4.

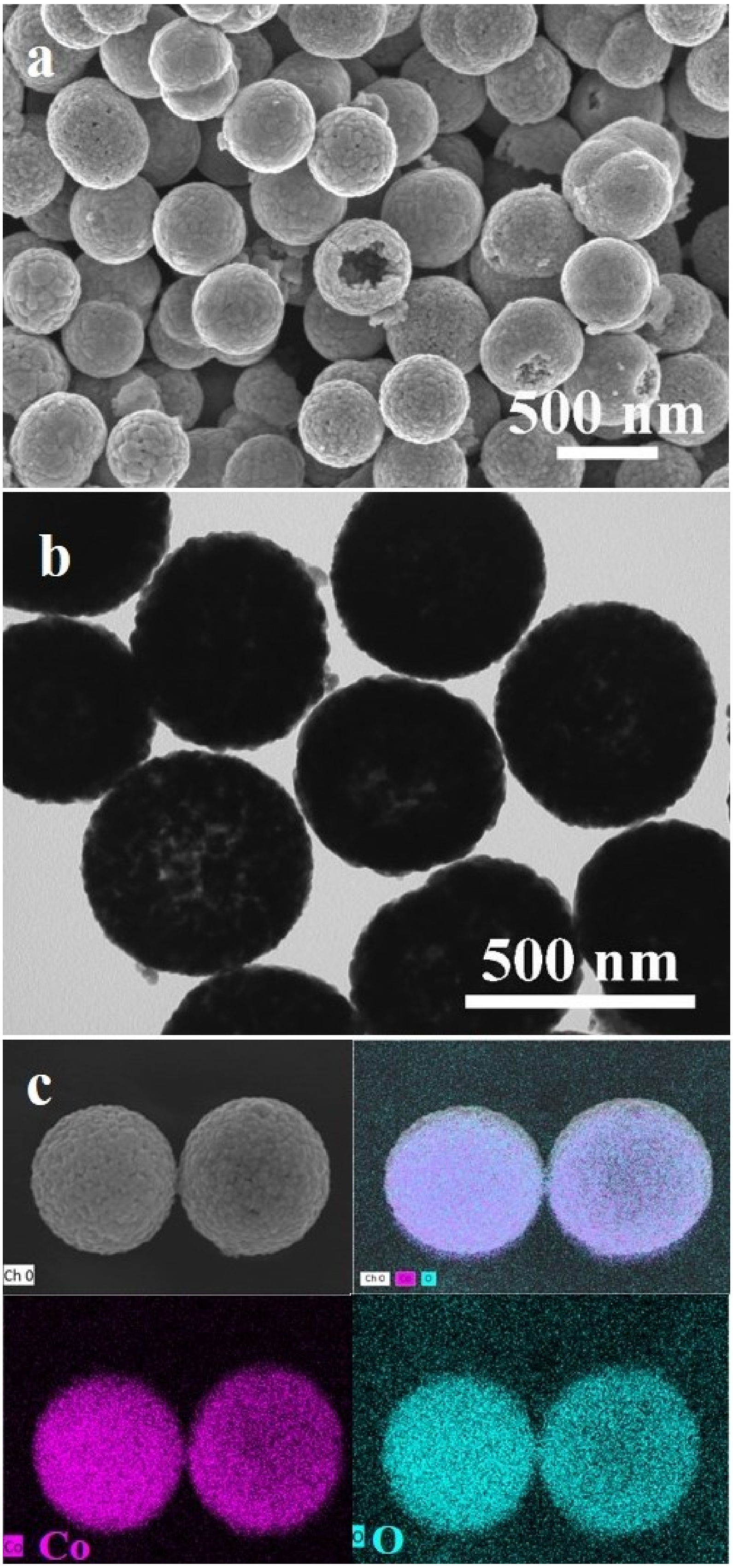

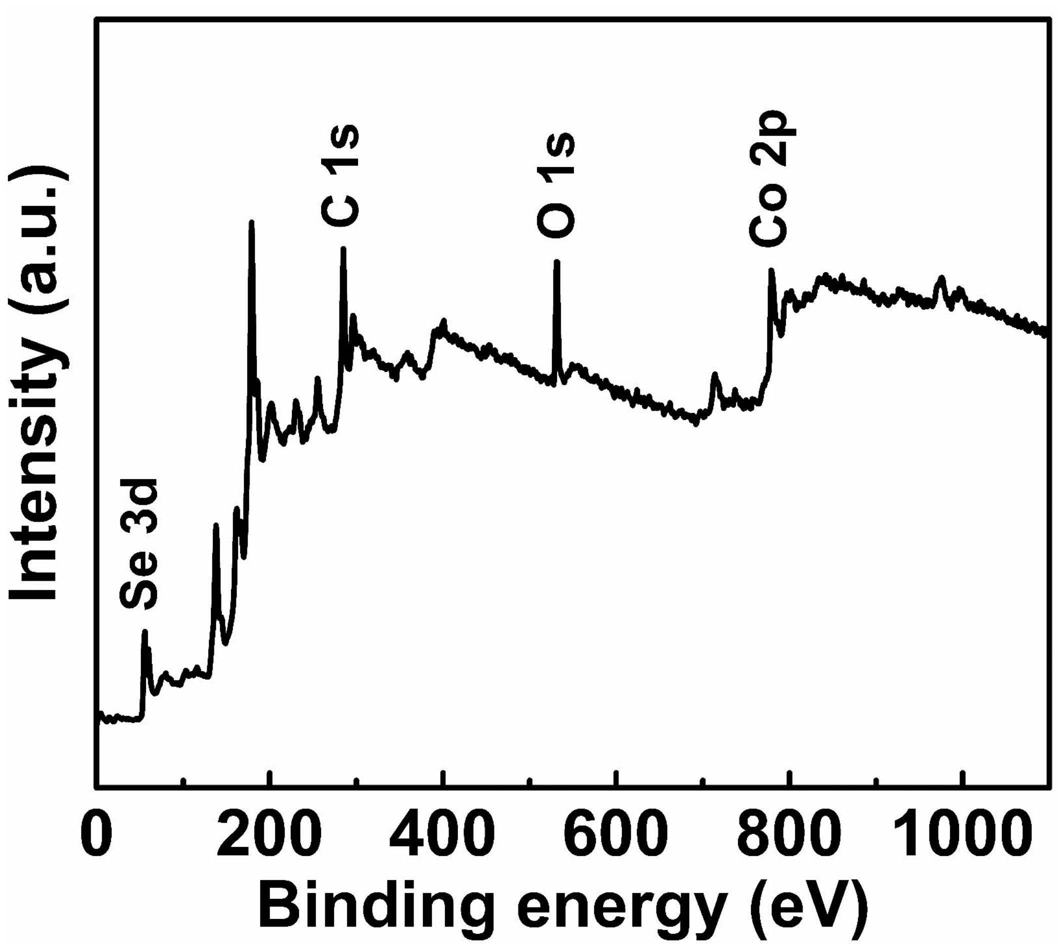

Fig. S6 XPS spectrum of $CoSe_2$/C.

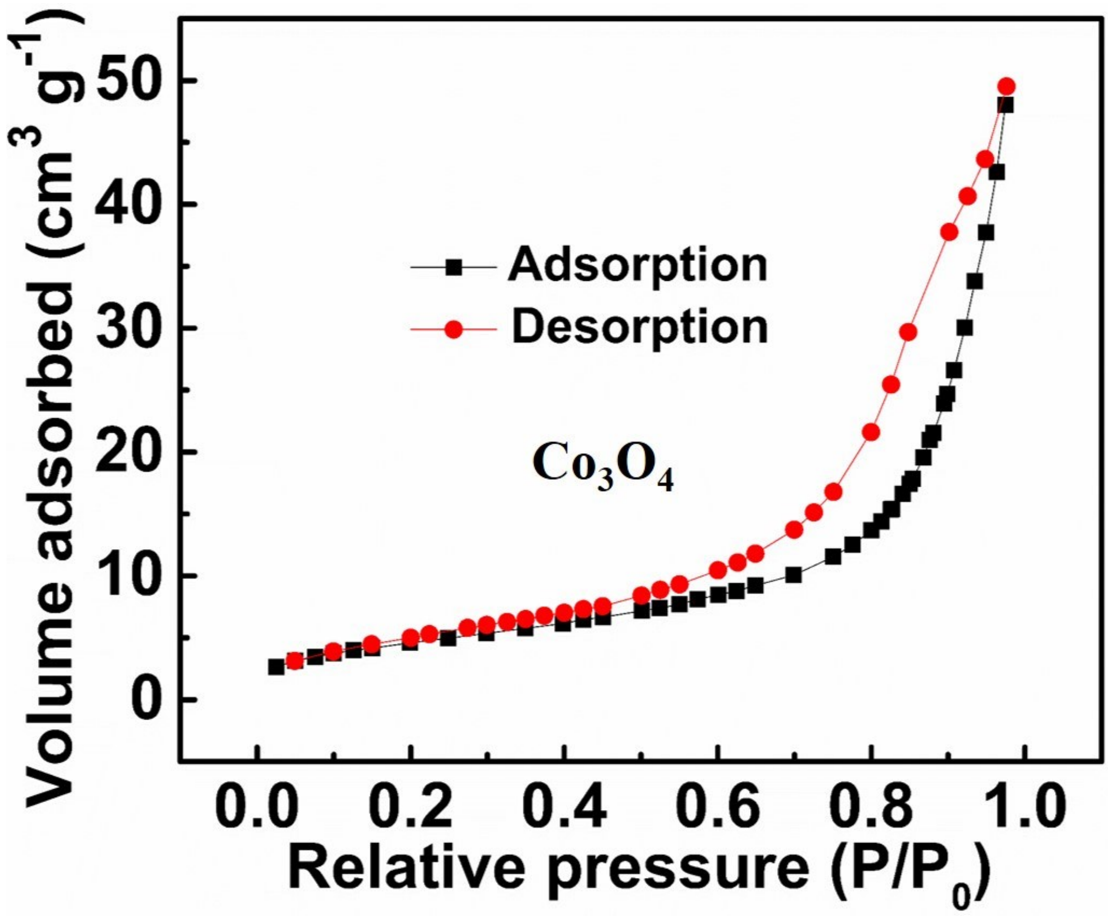

Fig. S7 N_2 adsorption/desorption isotherms of Co_3O_4.

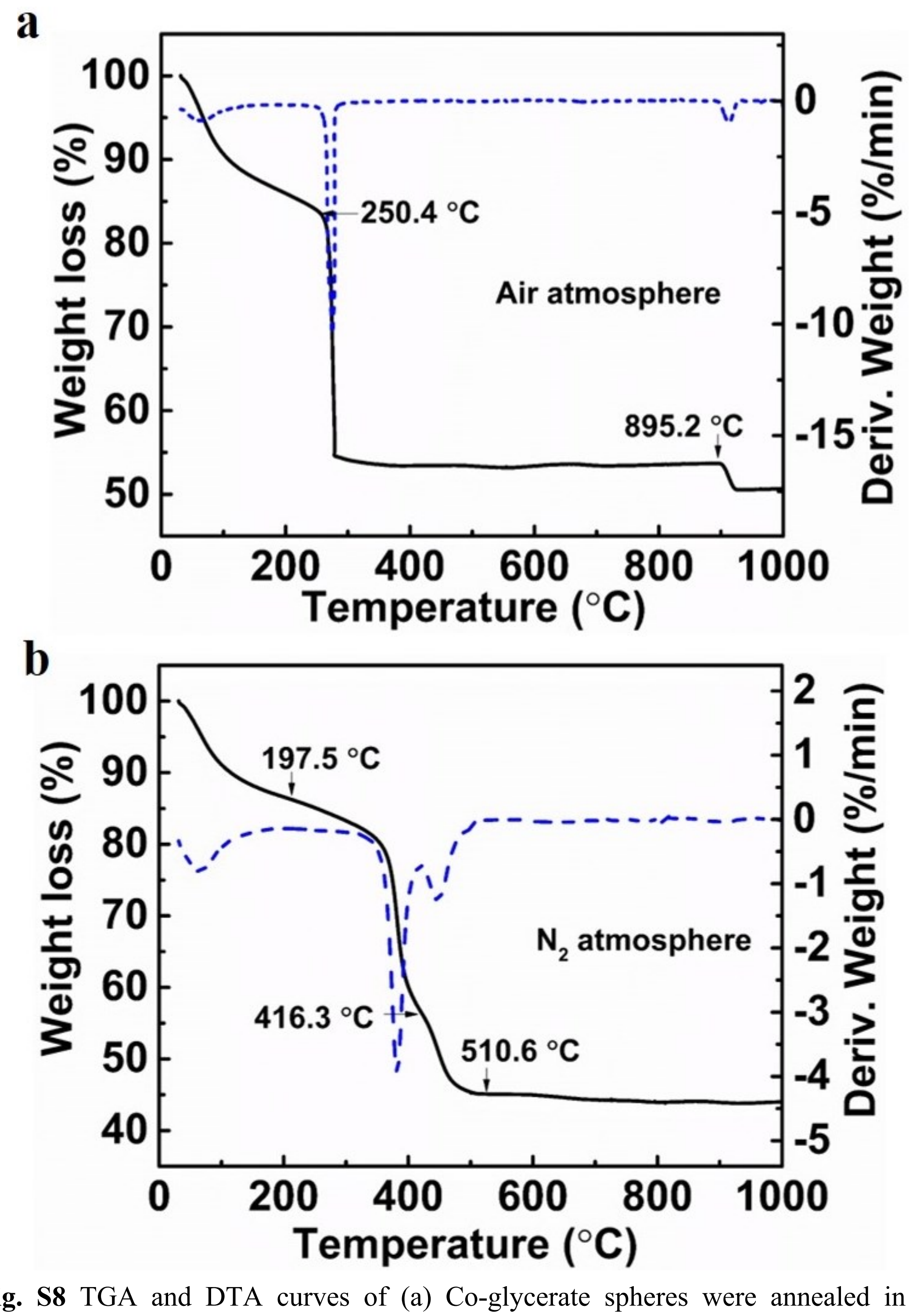

Fig. S8 TGA and DTA curves of (a) Co-glycerate spheres were annealed in air atmosphere, (b) Co-glycerate spheres were annealed in N_2 atmosphere.

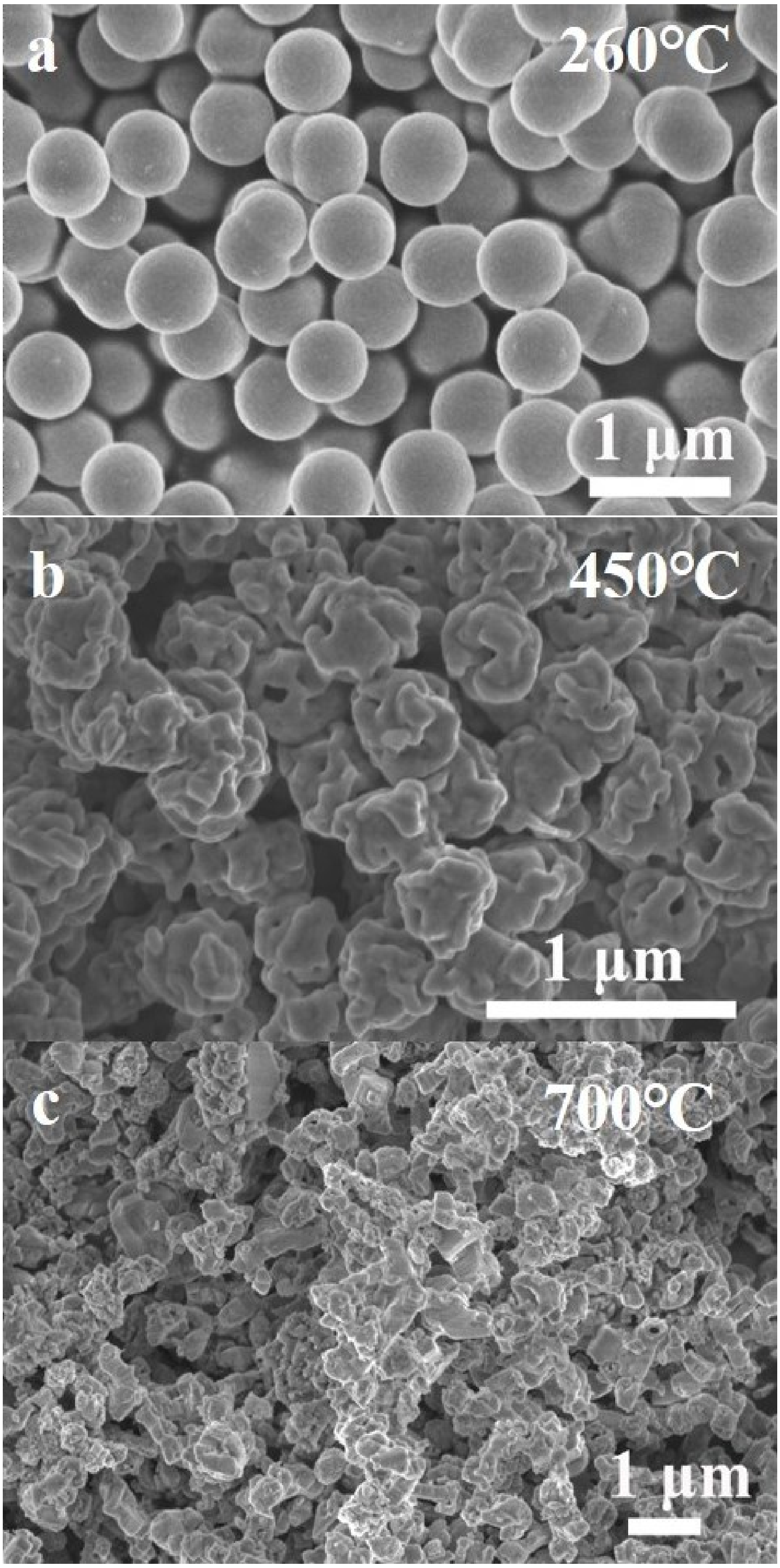

Fig. S9 FESEM images of (a, b, c) Co-glycerate spheres were annealed in N_2 atmosphere at different temperature.

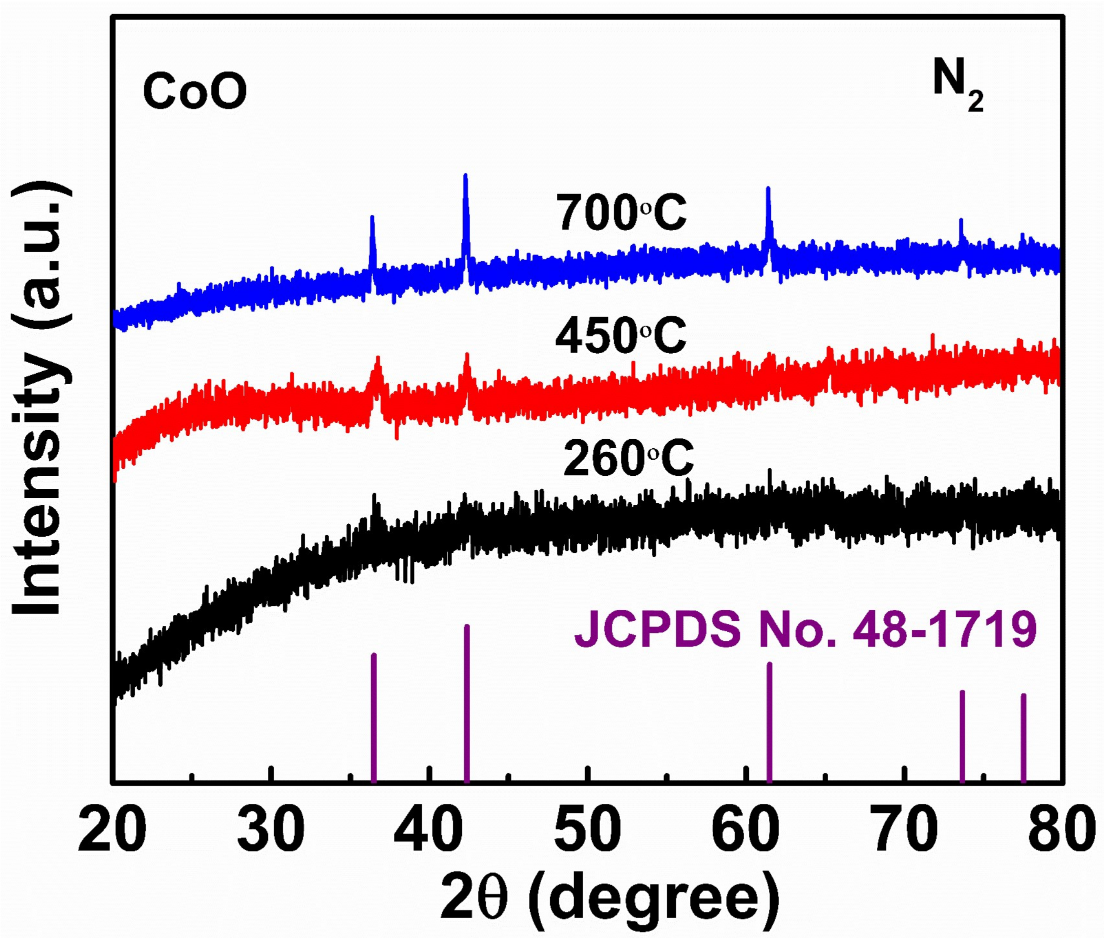

Fig. S10 XRD patterns of Co-glycerate spheres were annealed in N_2 atmosphere at different temperature.

Fig. S11 is placed above its caption.

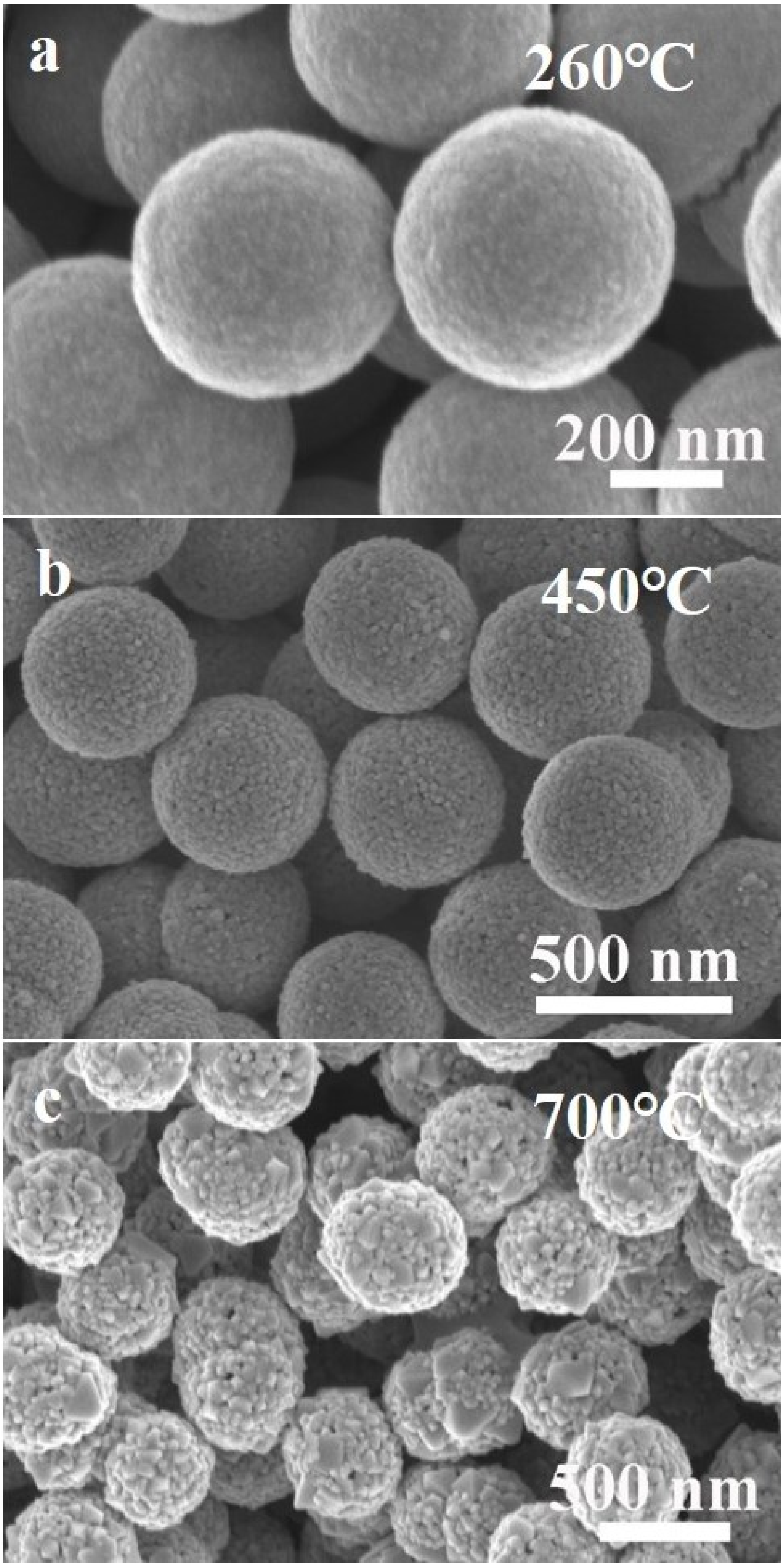

Fig. S11 FESEM images of (a, b, c) Co-glycerate spheres were annealed in air atmosphere at different temperature.

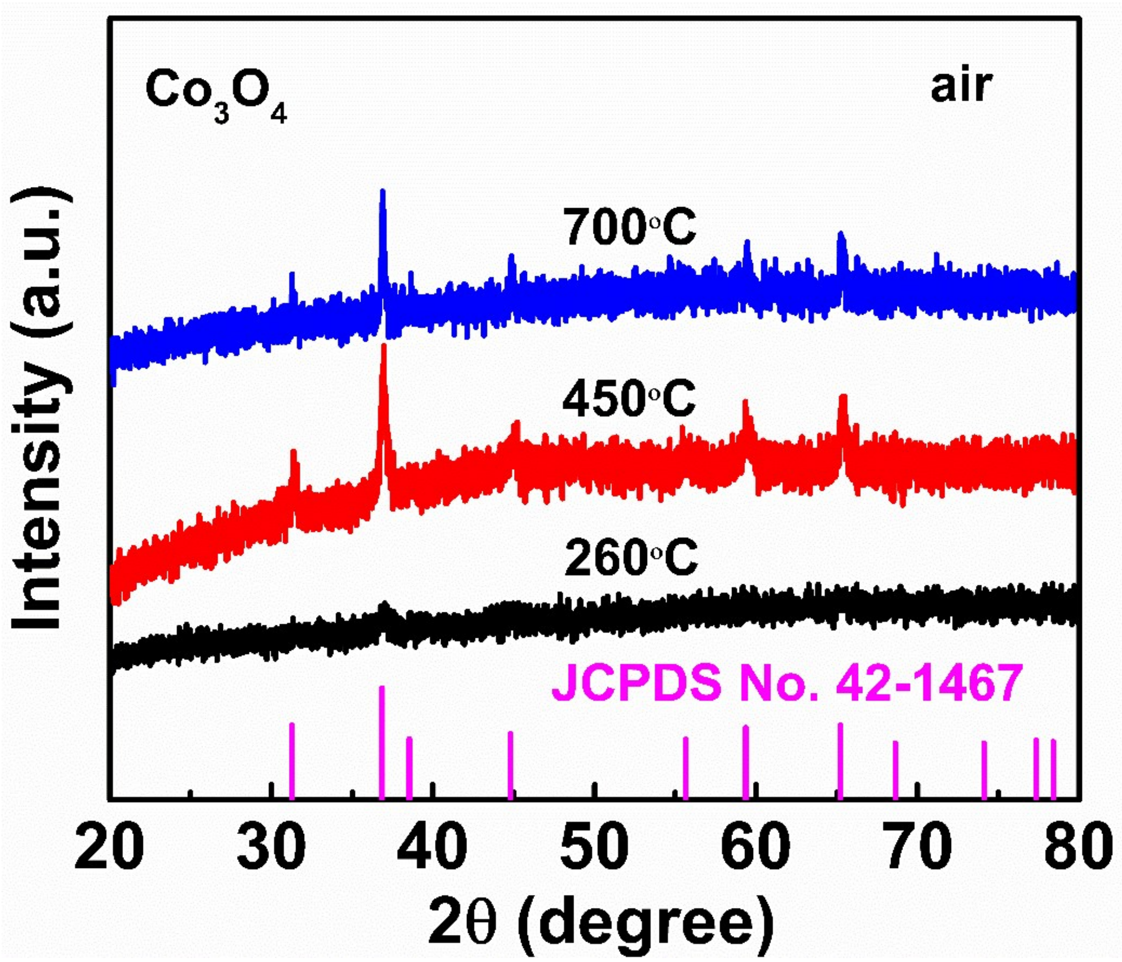

Fig. S12 XRD patterns of Co-glycerate spheres were annealed in air atmosphere at different temperature.

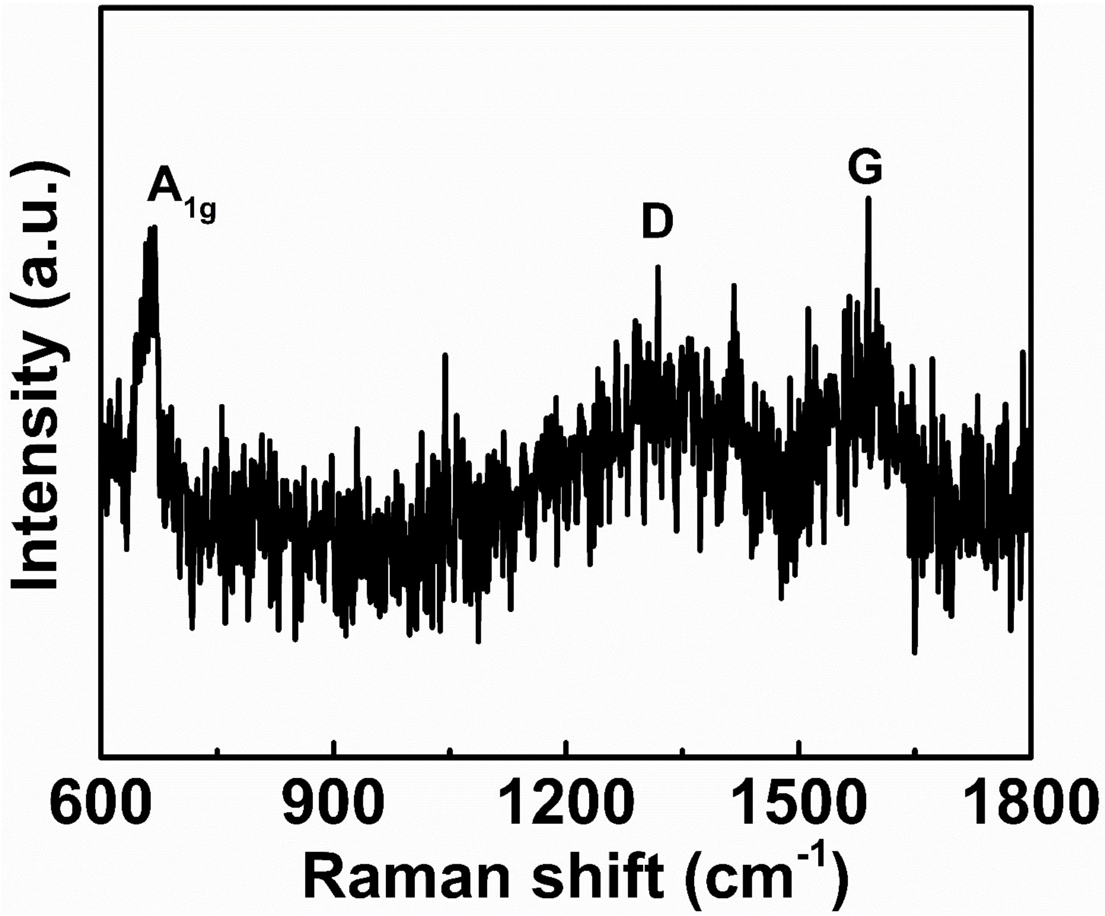

Fig. S13 Raman spectrum of $CoSe_2$/C.

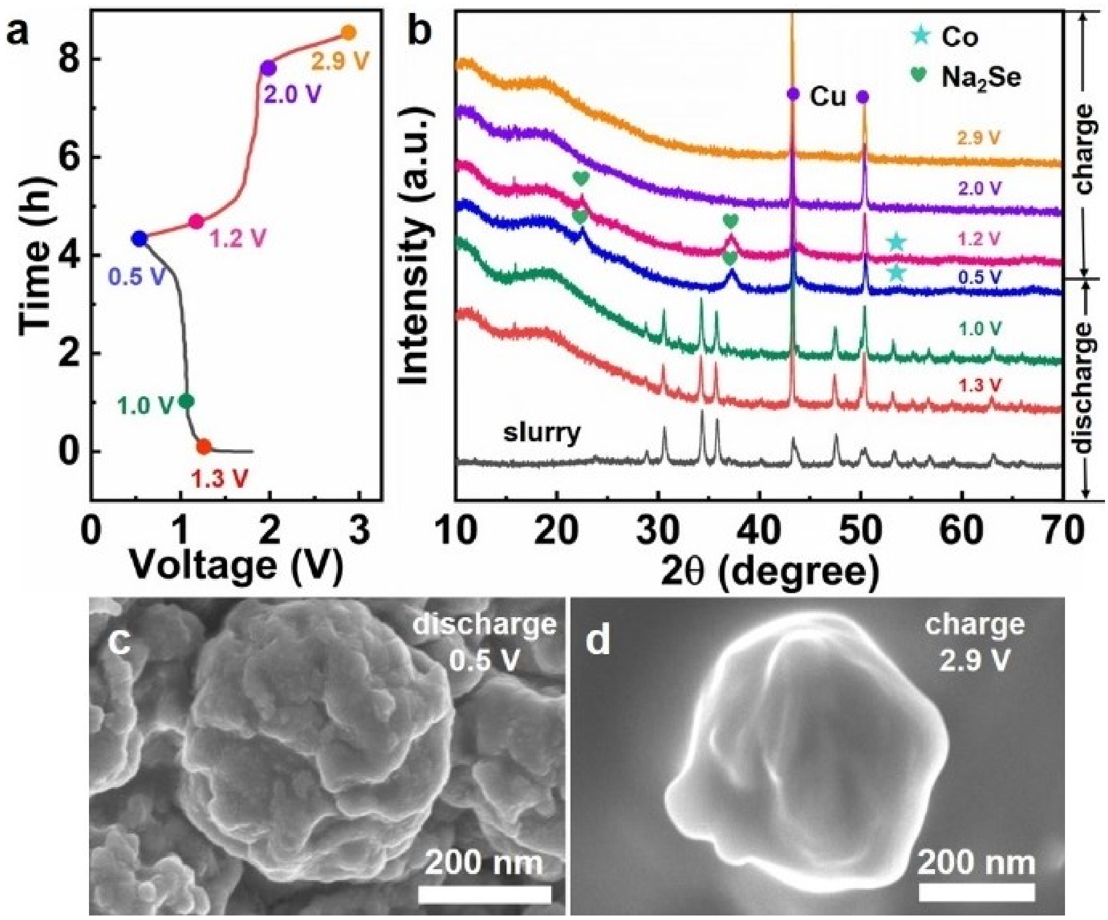

Fig. S14 (a) Charge-discharge curves of the first cycle at 100 mA g^{-1}, (b) ex-situ XRD patterns of $CoSe_2$/C for SIBs, SEM images of $CoSe_2$/C (c) discharge to 0.5 V, (d) charge to 2.9 V.

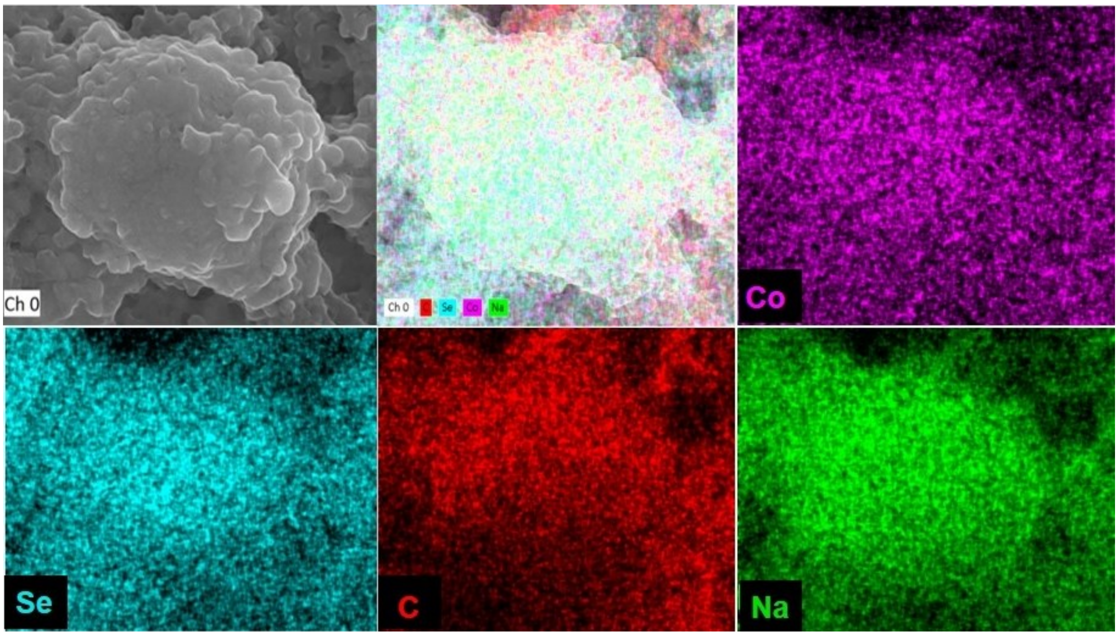

Fig. S15 Elemental mapping of $CoSe_2/C$ after 100 cycles at 500 mA g^{-1} for SIBs.

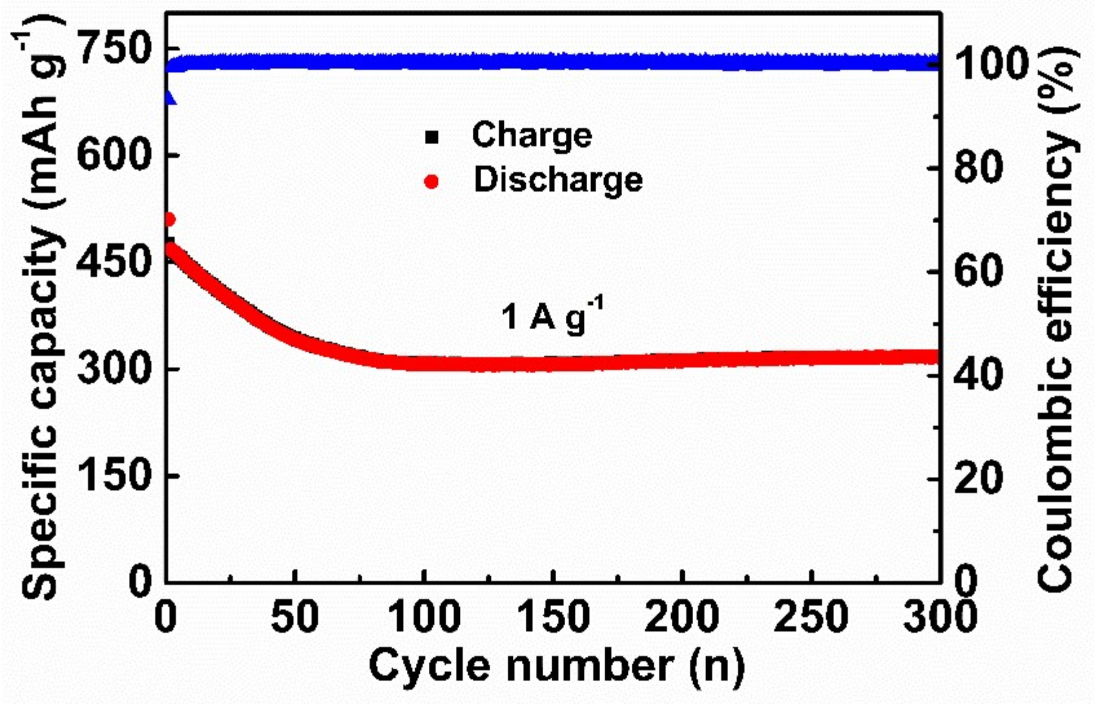

Fig. S16 Cycling performance of $CoSe_2$/C at 1 A g^{-1} in SIBs.

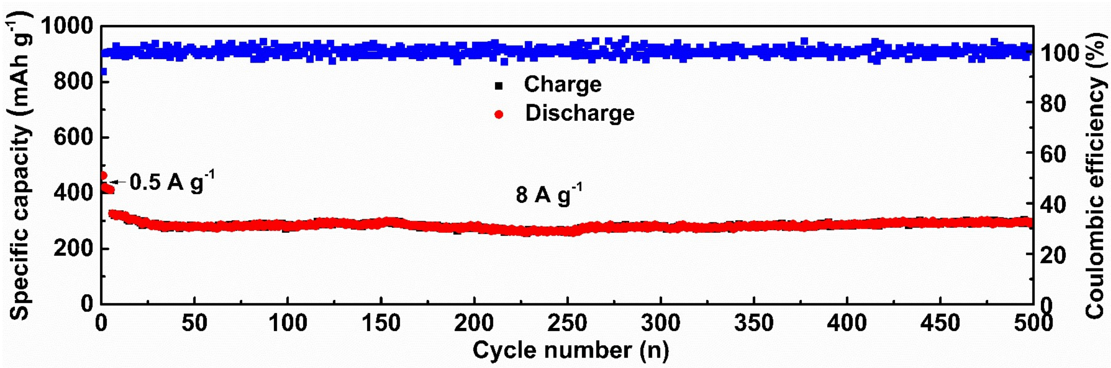

Fig. S17 Cycling performance of $CoSe_2$/C at 8 A g^{-1} in SIBs.

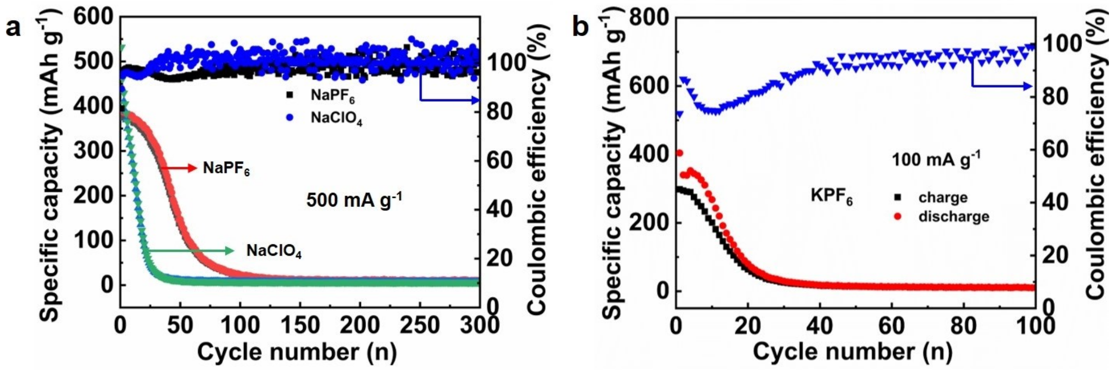

Fig. S18 The cycling performances at 500 mA g^{-1} in different electrolyte for SIBs (a) 1 M $NaClO_4$ in EC: DEC (1:1 Vol%) containing 5 wt.% FEC and 1 M $NaPF_6$ in EC: DEC (1:1 Vol%) containing 2 wt.% FEC, the cycling performances at 100 mA g^{-1} (b) 0.8 M KPF_6 in EC: DEC (1:1 Vol%) was used as electrolyte for PIBs.

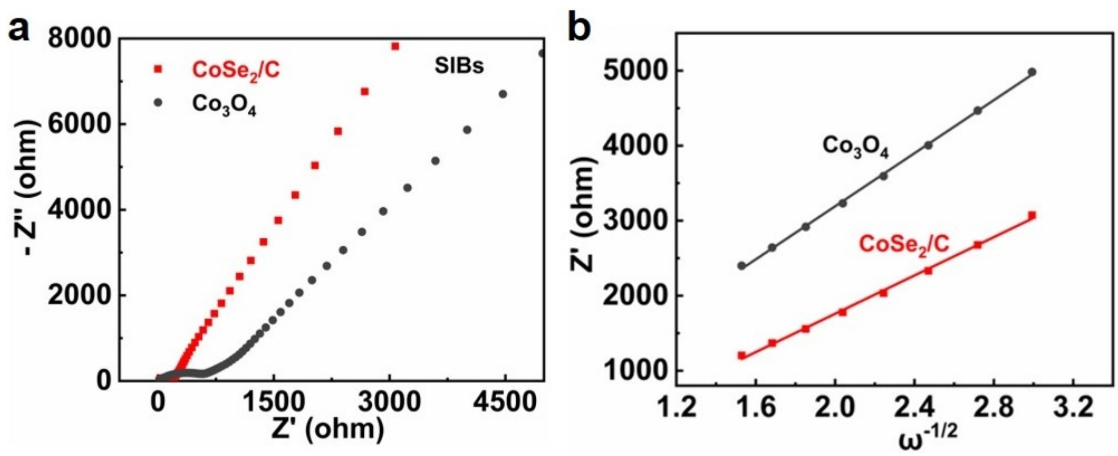

Fig. S19 (a) Electrochemical impedance spectra of $CoSe_2$/C and Co_3O_4 before cycle for SIBs, (b) The relationship between Z' and $\omega^{-1/2}$ for $CoSe_2$/C and Co_3O_4 in the low-frequency region.

a

b

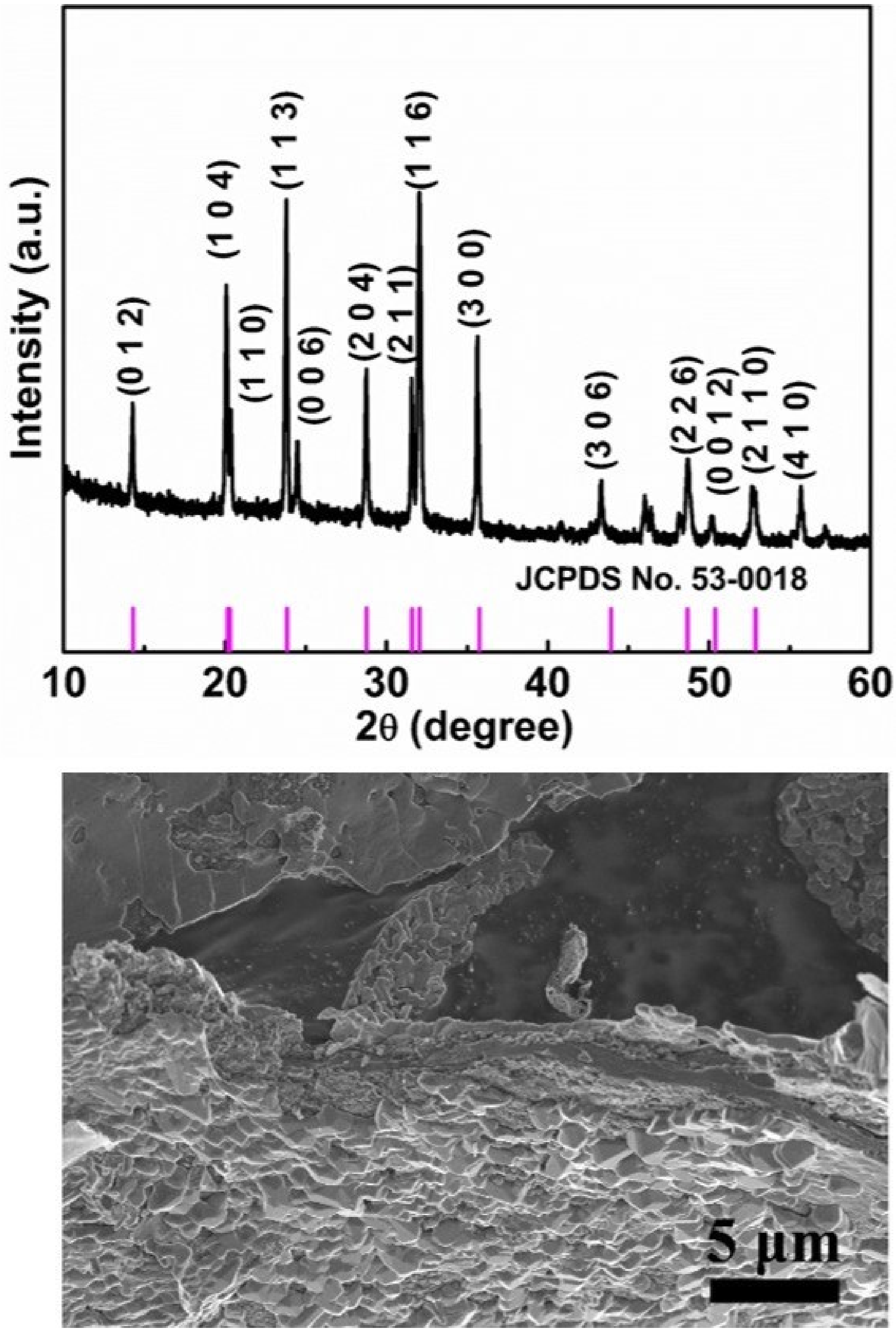

Fig. S20 (a) XRD pattern, (b) FESEM image of $Na_3V_2(PO_4)_3$@rGO.

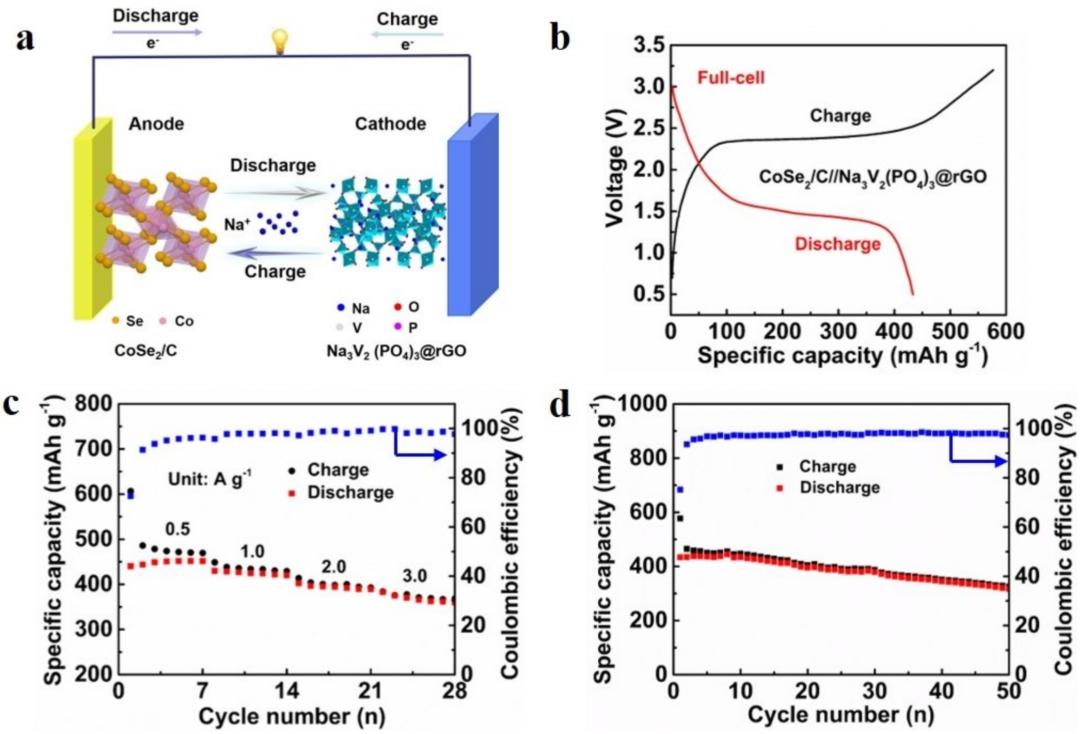

Fig. S21 (a) The working principle of SIBs full-cell with a $CoSe_2$/C anode and a $Na_3V_2(PO_4)_3$@rGO cathode, (b) charge-discharge curves of the 1st cycle at 1A g^{-1}, (c) rate performance, (d) cycling performances of $CoSe_2$/C//$Na_3V_2(PO_4)_3$@rGO in SIBs full-cell at 1 A g^{-1}.

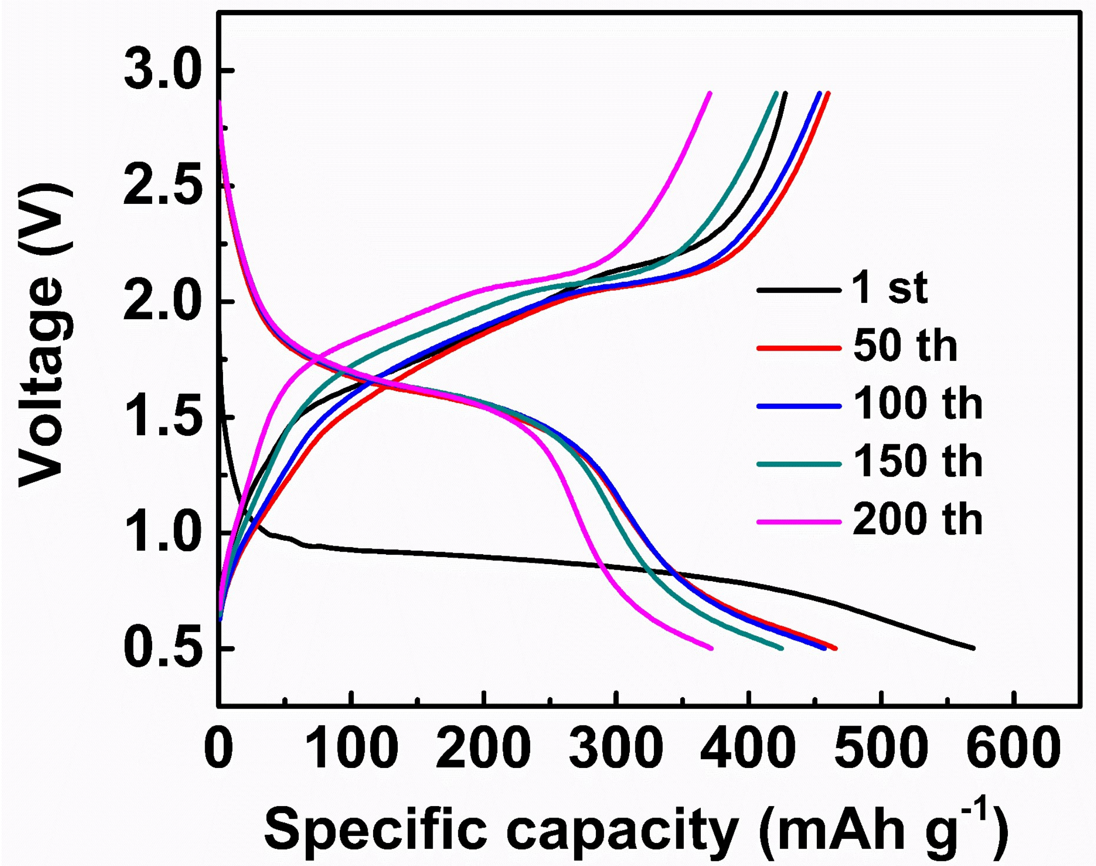

Fig. S22 Charge-discharge curves of $CoSe_2$/C at 50 mA g^{-1} in PIBs.

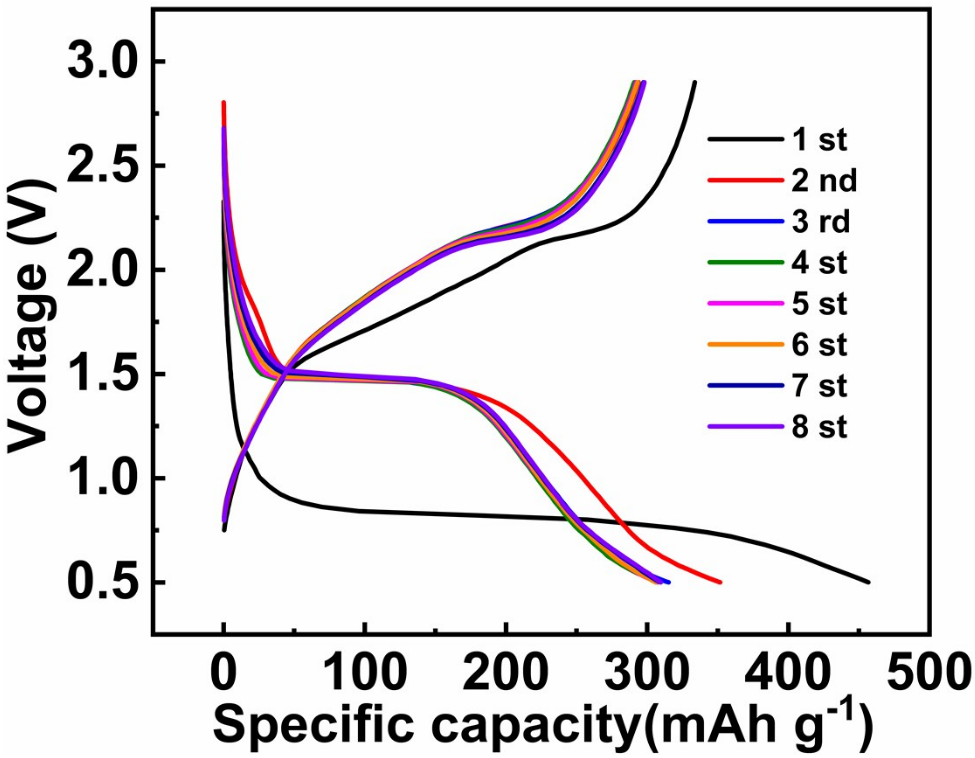

Fig. S23 When the mass load of $CoSe_2$/C was 6.3 mg cm^{-2} as anode for potassium ion battery, charge-discharge curves at 50 mA g^{-1}.

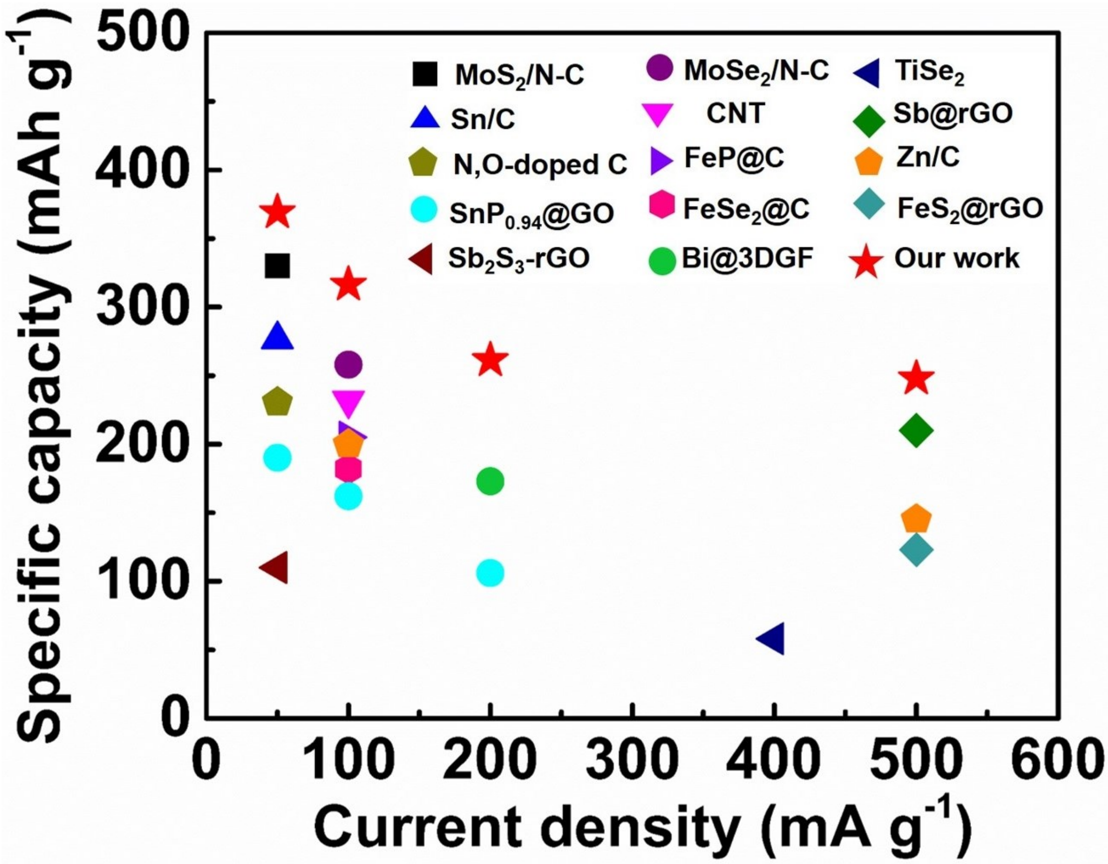

Fig. S24 Comparison the performance of $CoSe_2/C$ with recently reported materials in PIBs.

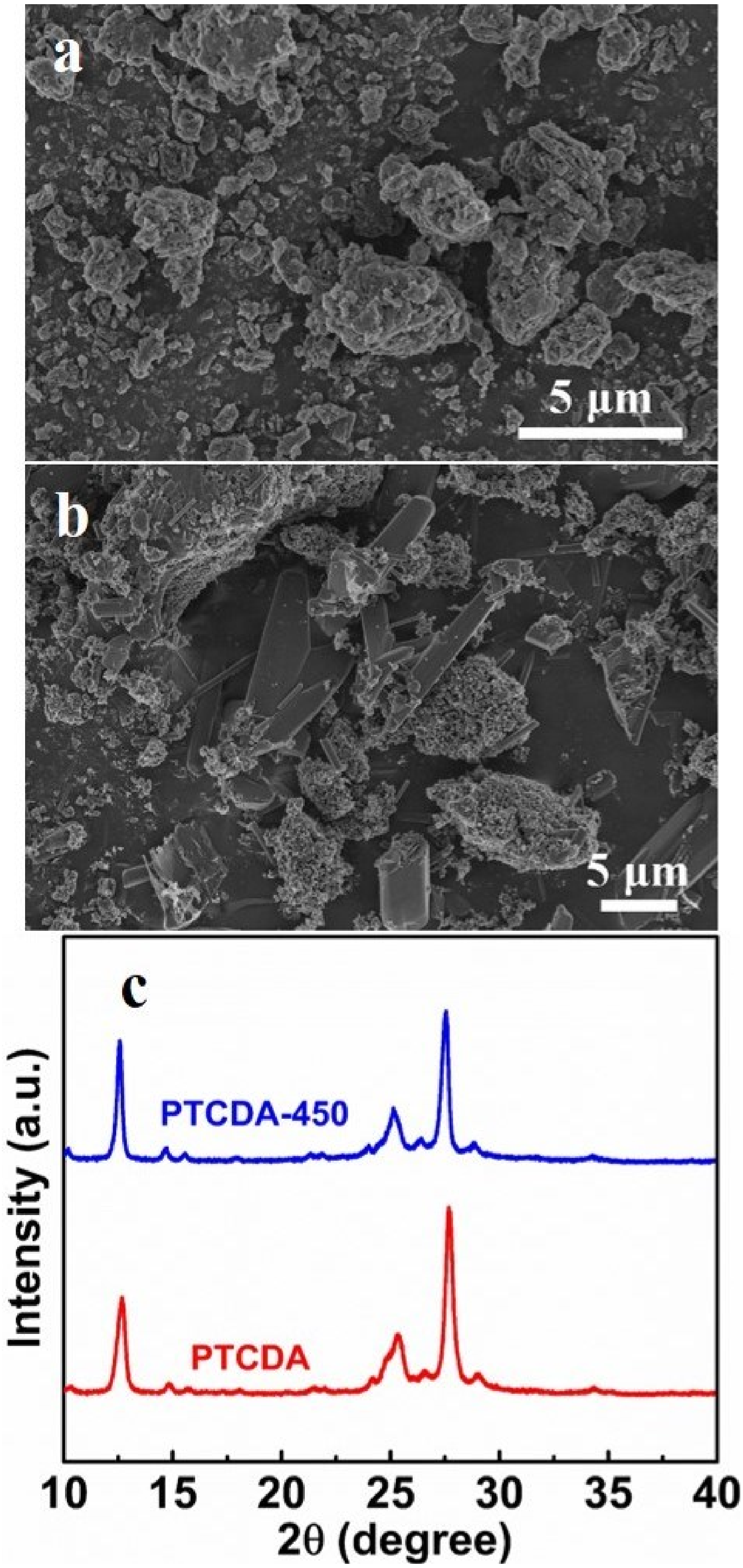

Fig. S25 FESEM images of (a) PTCDA, (b) PTCDA-450, (c) XRD patterns of PTCDA and PTCDA-450.

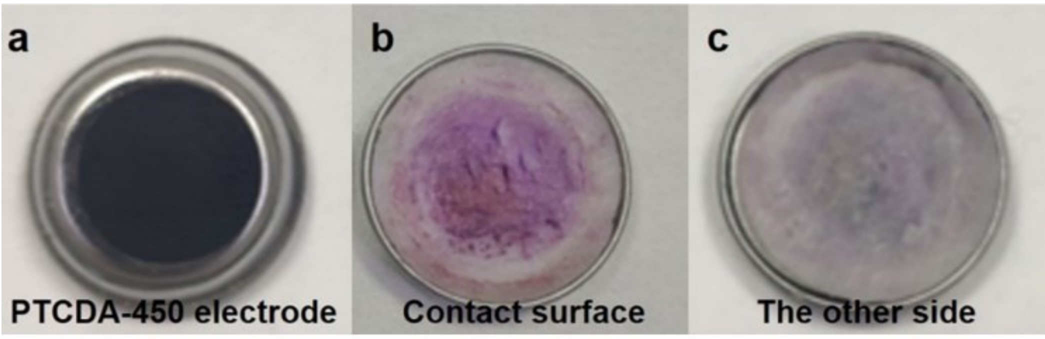

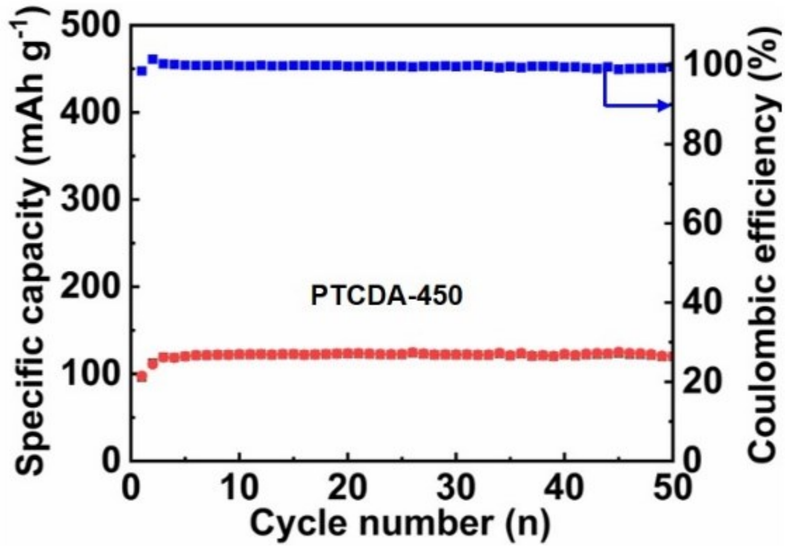

Fig. S26 Photos of disassembled battery after cycling (a) the electrode of PTCDA-450, (b) the side of separator contact with PTCDA-450 electrode directly, (c) the other side of separator, (d) the cycling performance of PTCDA-450 at 100 mA g^{-1} in half potassium ion battery.

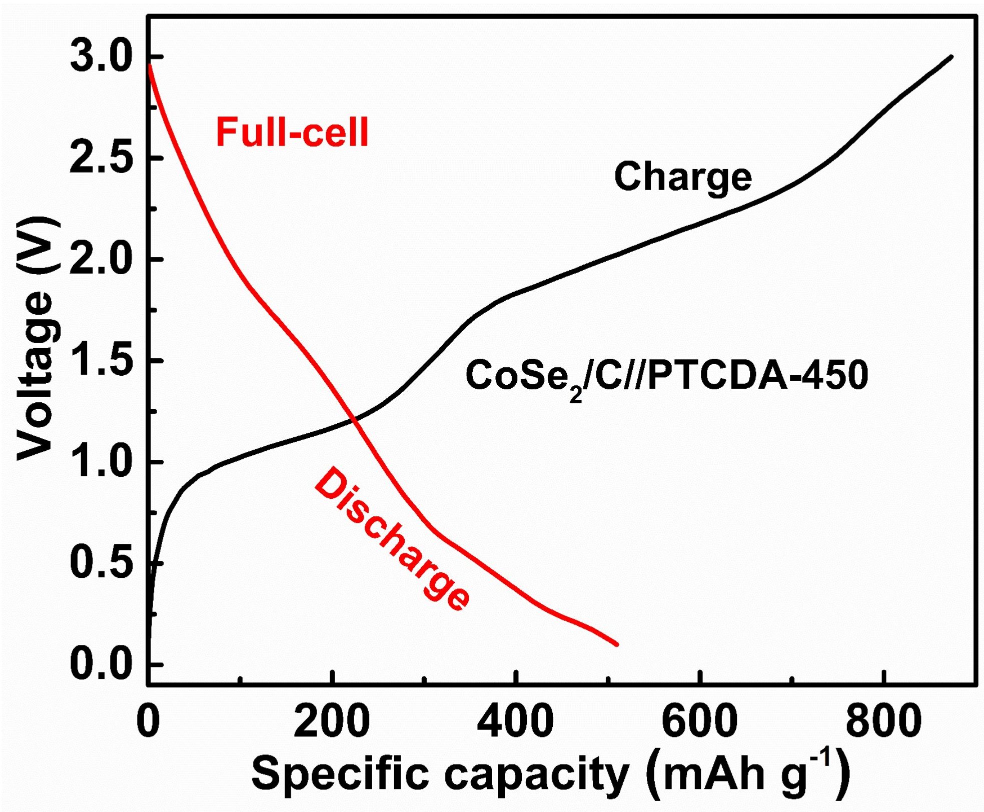

Fig. S27 The charge-discharge curves of $CoSe_2$/C//PTCDA-450 of the first cycle at 100 mA g^{-1} in PIBs full-cell.

Table S1. Comparison of electrochemical performance of $CoSe_2$/C with previous reported anode materials for PIBs.

Sample	Current density (mA g^{-1})	Cycle number	Reversible capacity (mAh g^{-1})	Ref.
MoS_2/N-C	50	50	330	1
Sn/C	50	100	276.4	2
N, O-doped C	50	100	230.6	3
$SnP_{0.94}$@GO	200	100	106	4
Sb_2O_3-rGO	50	50	110	5
$MoSe_2$/N-C	100	300	258.02	6
CNT	100	500	232	7
FeP@C	100	300	205	8
$FeSe_2$@C	100	100	182	9
Bi@3DGF	200	50	173	10
$TiSe_2$	400	300	~50	11
Sb@rGO	500	200	210	12
Zn/C-600	100	100	200	13
FeS_2@rGO	500	420	123	14
$CoSe_2$/C	50	200	369.2	This work
	100	200	316.4	This work
	200	200	261.3	This work
	500	200	248.1	This work
$CoSe_2$/C//PTCDA-450 (PIBs full-cell)	100	70	235.5	This work

Table S2. Comparison of electrochemical performance of $CoSe_2$/C with previous reported anode materials for SIBs.

Sample	Current density (A g^{-1})	Cycle number	Reversible capacity (mAh g^{-1})	Current density (A g^{-1})	Rate capacity (mAh g^{-1})	Ref.
$CoSe_2$@NC	0.2	200	374	6.4	~200	15
CNT/$CoSe_2$/C	~	~	~	2.4	223.6	16
$CoSe_2$@NC	2	1800	384.3	5	276.4	17
$CoSe_2$	1	1690	220	5	150	18
Cu-doped $CoSe_2$	1	500	~350	3	185	19
Ni_3S_2/Co_9S_8	0.1	100	419.9	2	323.2	20
NiS_2	0.5	100	186.9	0.5	209.8	21
$Fe_{1-x}S$	1	800	241.1	3.2	179.0	22
WSe_2/C	0.1	90	257.8	2	114.4	23
CuS	0.1	100	361.7	5	246.40.1	24
$MoSe_2$	1	200	360	5	281	25
$CoSe_2$/C	4	1600	312.1	3	322.0	This work
	8	500	297.6	5	292.8	
				8	266.5	
$CoSe_2$/C// $Na_3V_2(PO_4)_3$@ rGO (SIBs full-cell)	1	50	320.9	0.5	451.7	This work
				1.0	420.2	
				2.0	389.4	
				3.0	360.0	

References:

1 B. Jia, Q. Yu, Y. Zhao, M. Qin, W. Wang, Z. Liu, C.-Y. Lao, Y. Liu, H. Wu, Z. Zhang and X. Qu, *Adv. Funct. Mater.* 2018, **28**, 1803409.

2 K. Huang, Z. Xing, L. Wang, X. Wu, W. Zhao, X. Qi, H. Wang and Z. Ju, *J. Mater. Chem. A* 2018, **6**, 434-442.

3 J. Yang, Z. Ju, Y. Jiang, Z. Xing, B. Xi, J. Feng and S. Xiong, *Adv. Mater.* 2018, **30**, 1700104.

4 X. Zhao, W. Wang, Z. Hou, G. Wei, Y. Yu, J. Zhang and Z. Quan, *Chem. Eng. J.* 2019, **370**, 677-683.

5 V. Lakshmi, A. A. Mikhaylov, A. G. Medvedev, C. Zhang, T. Ramireddy, M. M. Rahman, P. Cizek, D. Golberg, Y. Chen, O. Lev, P. V. Prikhodchenko and A. M. Glushenkov, *J. Mater. Chem. A* 2020, **8**, 11424-11434.

6 J. Ge, L. Fan, J. Wang, Q. Zhang, Z. Liu, E. Zhang, Q. Liu, X. Yu and B. Lu, *Adv. Energy Mater.* 2018, **8**, 1801477

7 Y. Wang, Z. Wang, Y. Chen, H. Zhang, M. Yousaf, H. Wu, M. Zou, A. Cao and R. P. S. Han, *Adv. Mater.* 2018, **30**, 1802074.

8 F. Yang, H. Gao, J. Hao, S. Zhang, P. Li, Y. Liu, J. Chen and Z. Guo, *Adv. Funct. Mater.* 2019, **29**, 1808291.

9 T. Wang, W. Guo, G. Wang, H. Wang, J. Bai and B. Wang, *J. Alloys Compd.* 2020, **834**, 155265.

10 X. Cheng, D. Li, Y. Wu, R. Xu and Y. Yu, *J. Mater. Chem. A* 2019, **7**, 4913-4921.

11 P. Li, X. Zheng, H. Yu, G. Zhao, J. Shu, X. Xu, W. Sun and S. X. Dou, *Energy Storage Mater.* 2019, **16**, 512-518.

12 Z. Yi, N. Lin, W. Zhang, W. Wang, Y. Zhu and Y. Qian, *Nanoscale*, 2018, **10**, 13236-13241.

13 C. Yan, X. Gu, L. Zhang, Y. Wang, L. Yan, D. Liu, L. Li, P. Dai and X. Zhao, *J. Mater. Chem. A* 2018, **6**, 17371-17377.

14 J. Xie, Y. Zhu, N. Zhuang, H. Lei, W. Zhu, Y. Fu, M. S. Javed, J. Li, W. Mai, *Nanoscale*, 2018, **10**, 17092-17098.

15 B. Zhao, Q. Liu, G. Wei, J. Wang, X.-Y. Yu, X. Li and H. B. Wu, *Chem. Eng. J.* 2019, **378**, 122206.

16 M. Yousaf, Y. Chen, H. Tabassum, Z. Wang, Y. Wang, A. Y. Abid, A. Mahmood, N. Mahmood, S. Guo, R. P. S. Han and P. Gao, *Adv. Sci.* 2020, **7**, 1902907.

17 T. Liu, Y. Li, S. Hou, C. Yang, Y. Guo, S. Tian and L. Zhao, *Chem.* 2020, DOI: 10.1002/chem.202000072.

18 X. Ma, L. Zou and W. Zhao, *Chem. Commun.* 2018, **54**, 10507-10510.

19 Y. Fang, X. Y. Yu and X. W. Lou, *Adv. Mater.* 2018, **30**, 1706668.

20 X. Liu, F. Zou, K. Liu, Z. Qiang, C. J. Taubert, P. Ustriyana, B. D. Vogt and Y. Zhu, *J. Mater. Chem. A*, 2017, **5**, 11781-11787.

21 K. J. Zhu, G. Liu, Y. J. Wang, J. Liu, S. T. Li, L. Y. Yang, S. L. Liu, H. Wang and T. Xie, *Mater. Lett.* 2017, **197**, 180-183.

22 S. Zhang, J. Mi, H. Zhao, W. Ma, L. Dang and L. Yue, *J. Alloys Compd.* 2020, **842**, 155642.

23 J. Li, S. Han, J. Zhang, J. Xiang, X. Zhu, P. Liu, X. Li, C. Feng, B. Xiang and M. Gu, *J. Mater. Chem. A*, 2019, **7**, 19898-19908.

24 L. Wu, J. Gao, Z. Qin, Y. Sun, R. Tian, Q. Zhang and Y. Gao, *J. Power Sources*, 2020, **479**, 228518.

25 Q. Su, X. Cao, T. Yu, X. Kong, Y. Wang, J. Chen, J. Lin, X. Xie, S. Liang and A. Pan, *J. Mater. Chem. A*, 2019, **7**, 22871-22878.